PHYSICAL REVIEW LETTERS

Preservation of Energy-Time Entanglement in a Slow Light Medium

Curtis J. Broadbent, Ryan M. Camacho, Ran Xin, and John C. Howell

Department of Physics and Astronomy, University of Rochester, Rochester, New York 14627, USA
(Received 5 December 2007; published 4 April 2008; corrected 7 April 2008)

We demonstrate the preservation of entanglement of an energy-time entangled biphoton through a slow light medium. Using the D_1 and D_2 fine structure resonances of Rubidium, we delay one photon of the 1.5 THz biphoton by ~ 1.3 correlation lengths and measure the fourth order correlation fringes. After the group delay the fringe visibility is reduced from $97.0 \pm 4.4\%$ to $80.0 \pm 4.8\%$, but is still sufficient to violate a Bell inequality. We show that temporal broadening is the primary mechanism for reducing the fringe visibility and that smaller bandwidths lead to greatly reduced broadening.

Temporal control of the properties of qubits is a significant challenge in the quest for practical quantum information processing (QIP). For photons, or "flying qubits", their temporary storage in a quantum memory can facilitate many applications (e.g., linear optics quantum computing [1]). Quantum memories have varying design requirements depending on the application. These range from the most stringent requirements of on-demand retrieval of stored qubits to simpler passive but tunable temporary qubit buffers. Here we investigate entanglement preservation of an energy-time entangled biphoton in a double resonance slow light medium. We show that it can be used as a passive, tunable qubit buffer.

Different types of quantum memories for photons have been investigated, each with its own strengths. Cyclical free-space memories for photonic qubits using Pockel cells have been demonstrated experimentally [2,3]. Cyclical fiber-based memories have also been proposed [4]. Both are well suited to QIP applications with a master clock cycle. Memories using Raman transitions and dark-state polaritons [5] in atomic ensembles have been extensively studied [6–10]. While extremely versatile, these types of memories often suffer from the difficulty of efficiently isolating and detecting single photons in the presence of strong coupling beams.

In this Letter we report on the buffering of a single photon from an entangled pair in a slow light medium and show that entanglement is preserved. We use the fine structure resonances of Rubidium to delay the amplitude of a single photon with a correlation bandwidth of 1.5 THz by ~ 1.3 correlation lengths. We observe a post-selected fourth order correlation fringe visibility of $80.0 \pm 4.8\%$ (reduced from $97.0 \pm 4.4\%$) for an energy-time entangled biphoton. This exceeds the value of 70.7% needed to violate a Bell inequality and demonstrates the preservation of entanglement. Additionally, we demonstrate that broadening is the primary mechanism responsible for the reduction of fringe visibility.

The fourth order correlation fringes are created with a Franson interferometer, a useful tool in the analysis of energy-time entanglement [11–13]. It consists of two Michelson interferometers with highly unbalanced arm lengths so that no single photon interference occurs (see Fig. 1). Inserting a photon from an energy-time entangled biphoton into each Michelson interferometer and then scanning one of the four arms results in interference fringes in the detected coincidences. The fringes arise due to spectral correlations between the entangled photons. The visibility of these interference fringes can be used to verify the presence of entanglement [14,15]. By inserting a slow light medium into one arm of one of the interferometers, we delay the photon probability amplitude traveling in that path. The delay can be measured by observing a shift in the location of the Franson fringes. Additionally, the reduction of entanglement can be observed via the reduction of fringe visibility and the elongation of the fringe envelope due to group velocity dispersion of the photons in the slow light medium.

The energy-time entangled pair is generated with spontaneous parametric down-conversion (SPDC). The unnormalized SPDC quantum state for an extremely narrow band pump is given by

$$|\Psi\rangle \propto \int d\omega [f_s f_i \phi](\omega) \hat{a}_1^\dagger(\omega) \hat{a}_2^\dagger(\omega_p - \omega)|0\rangle, \quad (1)$$

where $\phi(\omega)$ describes the phase-matching constraints for collinear down-conversion [16], and the functions $f_s(\omega)$ and $f_i(\omega)$ represent any filtering or dispersion (e.g., in
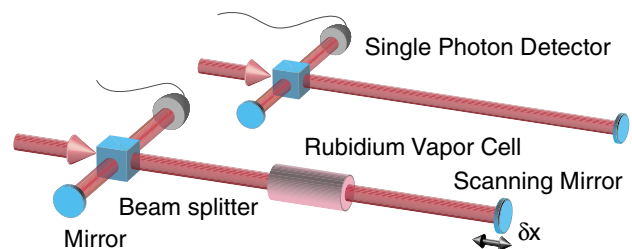

FIG. 1 (color online). Interferometric setup. Two unbalanced Michelson interferometers are used to measure the delay and preservation of entanglement of a photon traversing the heated Rb vapor cell slow light medium.

fiber) encountered by the signal and idler photons before entering the Franson interferometer.

By evolving the creation operators of the biphoton state through the Franson interferometer we arrive at

$$|\Psi_F\rangle \propto \int d\omega [f_s f_i \phi](\omega)(e^{-2i(\omega_p - \omega)t_{12}} + e^{-2i(\omega_p - \omega)t_{22}})$$

$$\times (e^{-2i\omega t_{11}} + e^{-2i(\omega(t_{21} - \tau + \delta t) + n(\omega)\omega\tau)})$$

$$\times \hat{a}_1^\dagger(\omega)\hat{a}_2^\dagger(\omega_p - \omega)|0\rangle, \qquad (2)$$

where $n(\omega)$ is the Rb index of refraction, t_{jk} refers to the free-space optical path length of the jth arm of the kth Michelson interferometer, and $\tau = L_{\text{Rb}}/c$ indicates the length of the Rb vapor cell. $\delta t = \delta x/c$ refers to the translation of the mirror in the interferometer arm containing the slow light medium as shown in Fig. 1.

In the Franson interferometer, the interference fringes arise from photons detected simultaneously. The interference is a result of the relative phase between the biphoton probability amplitudes which represent the short-short [ss] and long-long [ll] interferometer paths. Consequently, we post-select the simultaneous coincidences (by ignoring the short-long and long-short cross terms) to arrive at

$$|\Psi_F\rangle \propto \int d\omega [f_s f_i \phi](\omega)(1 + e^{-2i\{\omega[\delta t + (n-1)\tau] + \omega_p \Delta t\}})$$

$$\times \hat{a}_1^\dagger(\omega)\hat{a}_2^\dagger(\omega_p - \omega)|0\rangle, \qquad (3)$$

where we have taken $t_{j1} = t_{j2}$ for simplicity, and where $\Delta t = t_{2k} - t_{1k}$ is the common path mismatch. When first introduced, the functions $f_s(\omega)$ and $f_i(\omega)$ represented only the dispersion and filtering prior to the interferometer; however, we note that the form of Eq. (3) indicates that they may also be taken to include any dispersion or filtering which occurs after the interferometer before detection.

Since the experimental coincidence window, ~3 ns, is much larger than the biphoton correlation time, $\tau_b \simeq$ 685 fs, and smaller than twice the common path mismatch, $2\Delta t \simeq 6$ ns, the ss/ll coincidence rate R is given by

$$R \propto \iint dt' dt'' |\langle 0|\hat{E}_2^{(+)}(t'')\hat{E}_1^{(+)}(t')|\Psi_F\rangle|^2. \qquad (4)$$

We have assumed that the detectors have a flat spectral response so that the field operators are defined as

$$\hat{E}_j^{(+)}(t) \propto \int d\omega_j e^{-i\omega_j t}\hat{a}_j(\omega_j). \qquad (5)$$

The coincidence rate can then be reduced to

$$R(\tau) \propto \int d\omega |f_s(\omega)|^2 |f_i(\omega)|^2 \phi^2(\omega)\xi(\omega), \qquad (6)$$

where

$$\xi(\omega) = 1 + e^{4n_i(\omega)\omega\tau} + 2e^{2n_i(\omega)\omega\tau}$$

$$\times \cos(2\{\omega[\delta t + (n_r - 1)\tau] + \omega_p \Delta t\}), \qquad (7)$$

with $n_r(\omega) = \text{Re}[n(\omega)]$, and $n_i(\omega) = \text{Im}[n(\omega)]$. The phase-matching function $\phi(\omega) = \text{sinc}[(\tilde{n}_{gs} - \tilde{n}_{gi}) \times (\omega - \omega_{s0})L_c/2c]$, is given in terms of the crystal length, L_c, and the signal and idler crystal group indices, $\tilde{n}_{gs}$ and $\tilde{n}_{gi}$. In the case where the idler is sent through the slow light medium Eq. (6) still applies except that $\xi(\omega)$ is replaced by $\xi(\omega_p - \omega)$.

Examination of Eq. (6) and (7) reveals some remarkable aspects of the Franson interferometer. First, the visibility and fringe peak of Franson interference fringes are independent of any dispersion experienced outside of the interferometer (e.g., in optical fiber). Only the absolute value of $f_s(\omega)$ and $f_i(\omega)$ enter into Eq. (6). Consequently, in the following, $f_s(\omega)$ and $f_i(\omega)$ will only represent spectral filtering of the signal and idler photons. Secondly, as shown in Eq. (7), all orders of dispersion and attenuation introduced by the slow light medium contribute to the final form of the interference fringes.

Evaluation of the integral in Eq. (6) can be accomplished numerically with a suitable model for the index of the Rb vapor, $n(\omega)$. Including collisional broadening, the Rb vapor index of refraction can be modeled by

$$n(\omega) = 1 - \sum_{j=1}^{2} \frac{N|\mu_j|^2}{2\epsilon_0 \hbar} \sum_{k=1}^{4} \left(\frac{g_{jk}}{\omega - \omega_{jk} + i(\gamma_j + \gamma_c)} \right), \qquad (8)$$

where N and γ_c are the number density and collisional broadening full-width-half-maximum (FWHM) linewidth at temperature T. μ_j, g_{jk}, ω_{jk}, and $2\gamma_j$ correspond to the far detuned effective dipole moment, the relative peak strength, the resonance frequency, and the homogeneous FWHM linewidth, for the hyperfine resonances of the $j = \{1, 2\} \rightarrow \{D_1, D_2\}$ lines of ^{87}Rb and ^{85}Rb ($k = \{1, 2, 3, 4\} \rightarrow \{|^{87}\text{Rb}, F = 1\rangle, |^{87}\text{Rb}, F = 2\rangle, |^{85}\text{Rb}, F = 2\rangle, |^{85}\text{Rb}, F = 3\rangle\}$). In the present experiment, we use a pump laser centered at pump at $\lambda_p = 388$ nm and generate signal photons with a center wavelength of $\lambda_{s0} = 785$ nm and idler photons centered at $\lambda_{i0} = 767.2$ nm. By filtering the signal photons with a 3 nm filter we reduce the biphoton bandwidth to 1.5 THz. Actual line shapes are more accurately modeled by a Voigt profile, but since all photons are very far detuned from resonance (for example, the signal photon is detuned from the D_2 resonances by ~2.5 THz whereas the FWHM of the doppler valley is ~0.7 GHz) we ignore the rapidly decaying doppler contribution in the index model. The collisional broadening width is given by $\gamma_c(T) = 2\pi\sigma_0 v_{\text{rms}}(T)N(T)$ where, $\sigma_0 \simeq 2 \times 10^{-14}$ cm^{-2} is the Rb-Rb spin exchange cross section. All calculations presented in this Letter include collisional broadening.

Using the design spectrum of the 3 nm signal filter, $f_s(\omega)$, we have calculated the Franson fringes for three scenarios: (a) $L_{\text{Rb}} = 0$ cm, (b) $L_{\text{Rb}} = 10$ cm with the idler photon ($\lambda_{i0} = 767.2$ nm) sent through the interferometer

with the slow light medium, and (c) $L_{Rb} = 10$ cm with the signal photon ($\lambda_{s0} = 785$ nm) sent through the interferometer with the slow light medium. Though far outside the resonances, the idler photon will experience some delay when sent through the slow light medium due to the nonconstant index of refraction of the Rb vapor at the idler wavelength. The fringe envelopes were calculated with $T = 210\,°C$ and can be seen in Fig. 2.

By angle tuning 3 mm of BBO cut for type-II collinear SPDC we generate photons at the signal and idler wavelengths using a 100 mW cw pump laser at $\lambda_p = 388$ nm which has a bandwidth of 2 MHz. The signal and idler photons are separated at a polarizing beam splitter and coupled into single mode optical fibers (SMF). As previously mentioned, a 3 nm bandpass filter, $f_s(\omega)$, centered at 785 nm filters the signal photons before coupling into fiber. The idler photons are not filtered, $f_i(\omega) = 1$. Signal and idler photons then enter the fiber coupled Franson interferometer which has a common path mismatch of $\Delta t \sim 3$ ns. The long arm of interferometer 1 contains a 10 cm pyrex Rb vapor cell heated to $\sim 200\,°C$. The path length of the long arm in interferometer 1 is scanned using a 10 nm resolution translation stage. To reproduce the envelope of the fringes the stage is scanned with 50 nm steps over 1 μm at intervals of 20 μm. Near the center of the interference fringes the scanning is continuous for 20 μm with a 50 nm step size. The photons are detected with Perkin-

Elmer SPCM detectors (timing jitter ~ 600 ps) for 4 s at each location of the translation stage.

After the cell has been heated to a temperature of $\sim 200\,°C$, scenarios (b) and (c) discussed above are measured. Scenario (a) is not measured experimentally because removal of the pyrex vapor cell significantly alters the measured optical path length. In scenario (b) the idler photon is sent to the interferometer with the slow light medium and the fringes are measured. Then the fibers are then switched to measure scenario (c), where the signal photon centered at 785 nm is sent into interferometer with the slow light medium. Only polarization adjustment is used to rebalance the ss/ll count rates in the interferometer. The entire experiment is completed in ~ 120 min. Any turbulence during that time will only affect the phase over submicron length scales; thus, the fringe envelope is measured correctly even in the presence of interferometric instabilities.

Figure 2 also shows the measured Franson interference fringes. The visibility of the fringes for scenario (b), when the idler photon is sent through the interferometer containing the slow light medium, is $97.0 \pm 4.4\%$. The biphoton FWHM correlation length is $\tau_b \simeq 685$ fs as set by the 3 nm bandwidth of the 785 nm filter in the signal photon's beam path. The absolute peak-to-peak delay of the fringes with the slowed idler, scenario (b), relative to the fringes with the slowed signal, scenario (c), is $t_d \simeq 900$ fs, giving a fractional delay of $f_d = t_d/\tau_b \sim 1.3$. The fractional broadening, f_b, can be estimated by relating the FWHM of the interference fringes in scenario (b) and (c), which gives $f_b \sim 1.4$. The fringes resulting from sending the signal photon through the interferometer with the slow light medium, scenario (c), exhibit a visibility of $80.0 \pm 4.8\%$, demonstrating the preservation of entanglement.

The reduction of entanglement can be attributed to dispersive pulse broadening that arises as a result of the nonzero second and third order terms in an expansion of Rb index of refraction. The signal photons are significantly detuned from atomic resonances (≥ 2.5 THz), as noted above, causing absorption and absorptive broadening to be negligible. Dispersive pulse broadening can be drastically reduced by centering the pulse at the location where the second order terms in the index vanish, and by reducing the pulse bandwidth [17]. Though the fractional delay decreases linearly with the bandwidth, broadening falls off cubically, ultimately allowing larger absolute as well as fractional delays for narrow bandwidth pulses.

The largest absolute delay obtainable is limited by the creation of Rb_2 molecules which occurs at number densities upwards of $N \sim 10^{16}$ cm^{-3}, corresponding to $T \sim 350\,°C$. A high percentage of Rb_2 molecules changes the index profile and significantly increases the absorption and distortion of the delayed photon. With the signal wavelength at the zero second order dispersion wavelength, $\lambda_{s0} = 788.4$ nm, we calculate a maximum attainable delay
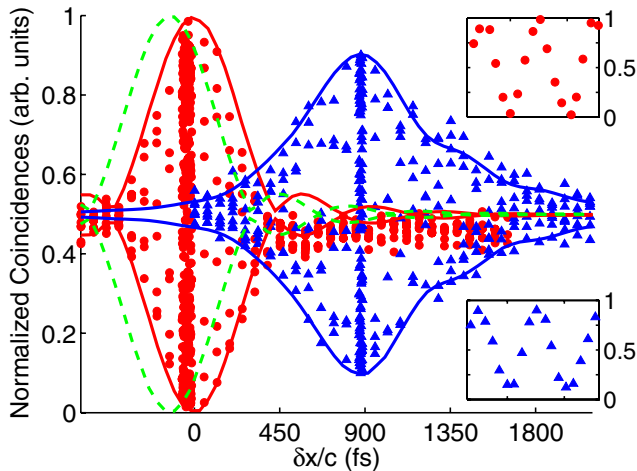

FIG. 2 (color online). Normalized interference data. The dotted and solid lines trace the calculated interference fringe envelopes for scenarios (a), (b), and (c), as noted in the text. The normalized measured coincidences for scenarios (b) and (c) are shown by the triangles and circles, respectively. Inset plots are close up views of the measured fringes near the center of each fringe envelope. The tick marks on the horizontal axes of the inset plots indicate the expected fringe period of λ_p/c. The maximum and minimum coincidence counts (M, m) for scenarios (b) and (c) are (998,15) and (631,70), respectively. Signal and idler singles rates (s, i) for scenarios (b) and (c) were (12,28) and (12,25) kHz, respectively.
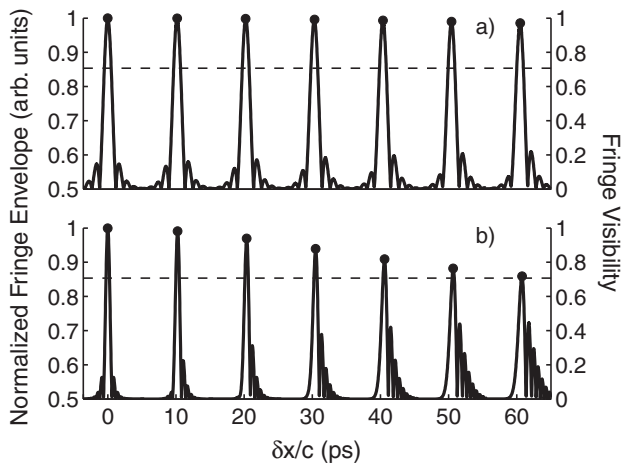
FIG. 3. Calculated interference fringe envelopes. Calculated normalized fringe envelopes vs delay for (a) $\sigma = 1$ nm and (b) $\sigma = 2$ nm for temperatures $T = 278, 304, 320, 332, 342,$ and $350\,°$C as compared to free-space fringes (left most envelope). The signal wavelength is at the zero second order dispersion wavelength, $\lambda_{s0} = 788.4$ nm. The dashed lines correspond to the Bell inequality visibility (right axis) of 70.7% as discussed in the text. The points indicate the visibility (right axis) of the corresponding envelope.

of roughly 60 ps at $T \sim 350\,°$C. The fractional delay f_d is consequently limited by the bandwidth of the biphoton and the loss of entanglement due to third order dispersive broadening. A fractional delay of $f_d \simeq 60$ can be achieved with a bandwidth of 2 nm; the visibility of the calculated Franson interference fringes in this case falls to 71.8% at $350\,°$C as shown in Fig. 3(b). With bandwidths narrower than ~ 1 nm, the visibility remains higher than 98% at $350\,°$C as can be seen in Fig. 3(a).

The delay mechanism demonstrated in this Letter may be applied to any double resonance structures and corresponding biphoton bandwidths. The ~ 200 MHz biphoton discussed in Ref. [18] should allow delays on the order of 100 ns (fractional delays of ~ 20) with relatively small pulse broadening as discussed in Ref. [17]. The cell temperature need only be $\sim 140\,°$C in this case; however, the loss would be quite large due to an increased optical depth resulting from the narrow 6.8 GHz hyperfine splitting. Regardless, such loss will be approximately spectrally flat for the narrow band photons leaving the entanglement largely unaffected.

While generating energy-time entangled biphotons with a cw pump laser may be of limited use for many QIP applications requiring well defined single photon wave packets or other types of entanglement (for example, polarization or transverse position-momentum entanglement), properly engineered double absorption resonance slow light media can still be expected to work effectively.

These types of slow light media have been shown to slow weak coherent light from a pulsed source, as well as to preserve the transverse wave vectors in a simple optical image [19]. Spectrally dependant Faraday rotation which would reduce polarization entanglement can be eliminated by passive and/or active magnetic shielding of the vapor cell.

In summary, we have demonstrated the tunable delay of one member of a pair of entangled photons relative to the other while preserving their entanglement. We sent an ensemble of 1.5 THz photons from energy-time entangled pairs into a hot Rubidium vapor and observed a shift of the fourth order correlation fringes by ~ 1.3 correlation lengths using the Rb D_1 and D_2 fine structure resonances. The $80.0 \pm 4.8\%$ visibility of the slowed fourth order correlation fringes violated a Bell inequality value by nearly 2 standard deviations, demonstrating the preservation of entanglement of the biphoton and preservation of the quantum state of the slowed photon. We examined the limitations of this particular method of slow light, calculating an absolute delay of 60 ps and a fractional delay of $f_d \simeq 60$ for a 1 THz photon, while still exceeding the Bell inequality value for the visibility of 70.7%.

[1] E. Knill, R. Laflamme, and G. J. Milburn, Nature (London) **409**, 46 (2001).
[2] T. B. Pittman, B. C. Jacobs, and J. D. Franson, Phys. Rev. A **66**, 042303 (2002).
[3] T. B. Pittman and J. D. Franson, Phys. Rev. A **66**, 062302 (2002).
[4] P. M. Leung and T. C. Ralph, Phys. Rev. A **74**, 022311 (2006).
[5] M. D. Lukin, Rev. Mod. Phys. **75**, 457 (2003).
[6] D. N. Matsukevich and A. Kuzmich, Science **306**, 663 (2004).
[7] A. V. Gorshkov et al., Phys. Rev. Lett. **98**, 123601 (2007).
[8] J. Nunn et al., Phys. Rev. A **75**, 011401(R) (2007).
[9] S. Chen et al., Phys. Rev. Lett. **97**, 173004 (2006).
[10] M. D. Eisaman et al., Nature (London) **438**, 837 (2005).
[11] J. D. Franson, Phys. Rev. Lett. **62**, 2205 (1989).
[12] P. G. Kwiat, A. M. Steinberg, and R. Y. Chiao, Phys. Rev. A **47**, R2472 (1993).
[13] J. Brendel et al., Phys. Rev. Lett. **82**, 2594 (1999).
[14] J. S. Bell, Physics **1**, 195 (1964).
[15] J. D. Franson, Phys. Rev. A **61**, 012105 (1999).
[16] R. Erdmann et al., Phys. Rev. A **62**, 053810 (2000).
[17] R. M. Camacho, M. V. Pack, and J. C. Howell, Phys. Rev. A **73**, 063812 (2006).
[18] Y. J. Lu and Z. Y. Ou, Phys. Rev. A **62**, 033804 (2000).
[19] R. M. Camacho, C. J. Broadbent, I. Ali-Khan, and J. C. Howell, Phys. Rev. Lett. **98**, 043902 (2007).